Bifurcation of quantum nonlinear resonances induced by a time-periodic vector potential

Suhan Ree and L. E. Reichl
Center for Studies in Statistical Mechanics and Complex Systems, The University of Texas at Austin, Austin, Texas 78712
(Received 5 August 1996)

The quantum mechanics of a two-dimensional ideal electron Fermi gas in a cylindrical cavity in the presence of a weak time-periodic vector potential is studied. Floquet eigenstates are obtained numerically and Husimi distribution functions are used to show the bifurcation and appearance of quantum nonlinear resonances. For electrons at the Fermi surface, if the frequency of the vector potential ω_0 is lower than a certain critical frequency ω_{cr} then there is no electron having a primary resonance. If ω_0 is higher than ω_{cr}, electrons with certain angular momenta will have primary resonances. [S1063-651X(97)03203-0]

PACS number(s): 05.45.+b, 03.65.Sq, 73.20.Dx

I. INTRODUCTION

The transition to chaos in classical systems occurs in regions of the classical phase space where self-similar sets of nonlinear resonances exist, grow, and overlap as a parameter of the system is changed. Nonlinear resonances have also been observed in the quantum counterpart of these systems, although they only form self-similar families down scales in the phase space of order $\hbar$ [1]. The effect of an underlying classical chaos on the quantum counterpart of these systems, especially systems with a periodic time-driven potential, is a topic that has received much attention recently. To investigate those systems quantum mechanically, the Floquet theory has been used [2–4].

The model we consider consists of a two-dimensional (2D) noninteracting electron gas confined by a circular hard wall of radius b. We will describe the system in cylindrical coordinates (r,ϕ). Because the system has circular symmetry, the angular momentum $\hat{p}_\phi$ of the electrons is a conserved quantity ($[\hat{H},\hat{p}_\phi]=0$). As a consequence, the system can be treated as a system with one degree of freedom, along the radial direction.

We can induce chaos in this system with a weak time-periodic radial vector potential. We can create the radial vector potential in the following manner. Let us assume the electron has mass m and charge e and at the center of the circular cavity there is a fiber of negligible radius a that has a weak confined alternating magnetic flux $\Phi_0\cos(\omega_0 t)$ with frequency ω_0. We assume that the only effect of the fiber is to provide a time-periodic vector potential in the circular two-dimensional cavity. It also imposes the boundary condition $\Psi(r=0,\phi)=0$ on the electron wave functions. We will ignore interactions between electrons. For small ω_0 $[(\omega_0/c)b\ll 1]$, the Schrödinger equation has the form

$$i\hbar\frac{\partial\Psi}{\partial t}=\left[\frac{[\hat{\mathbf{p}}-e\mathbf{A}(\hat{\mathbf{r}},t)]^2}{2m}+V_a(\hat{\mathbf{r}})+V_b(\hat{\mathbf{r}})\right]\Psi=\left[-\frac{\hbar^2}{2m}\frac{\partial^2}{\partial r^2}-\frac{\hbar^2}{2mr}\frac{\partial}{\partial r}-\frac{\left[\frac{\hbar}{i}\frac{\partial}{\partial\phi}-\beta\cos(\omega_0 t)\right]^2}{2mr^2}+V_a(r)+V_b(r)\right]\Psi, \quad (1)$$

where $\mathbf{A}=(\Phi_0/2\pi\hat{r})\cos(\omega_0 t)\mathbf{e}_\phi$, $\beta=e\Phi_0/2\pi$, and V_a and V_b are potentials associated with infinitely hard walls at $r=a$ and $r=b$. (See the Appendix for the classical Hamiltonian and the exact form of the vector potential of this model.)

In a previous paper [5] on the classical version of this system we found that the frequency ω_0 plays an important role in determining the manner in which chaos appears in the system. For a given classical angular momentum, as ω_0 increases there is a frequency at which nonlinear primary resonances start to emerge and also bifurcate immediately. The frequency ω_0 also determines the locations of primary resonances in phase space.

In Sec. II, we first obtain the energy eigenstates of the unperturbed system ($\beta=0$) and then use these to obtain the Floquet eigenstates of the full Hamiltonian of the model. Husimi plots of the Floquet states are used to compare results from classical and quantum mechanics. In Sec. III, properties of electrons with the Fermi energy are examined. Finally, in Sec. IV, we make some concluding remarks.

II. ONE-ELECTRON SYSTEM

A. Free Hamiltonian ($\beta=0$)

It is useful to study the free Hamiltonian $\hat{H}_0$ (when $\beta=0$) before considering the full Hamiltonian. The eigenstates of the unperturbed system are simultaneous eigenstates of the Hamiltonian $\hat{H}_0$ and the angular momentum $\hat{p}_\phi$. We denote the simultaneous eigenstates as $|l,n\rangle$ so that

$$\hat{H}_0|l,n\rangle=E_{l,n}|l,n\rangle, \quad \hat{p}_\phi|l,n\rangle=l\hbar|l,n\rangle. \quad (2)$$

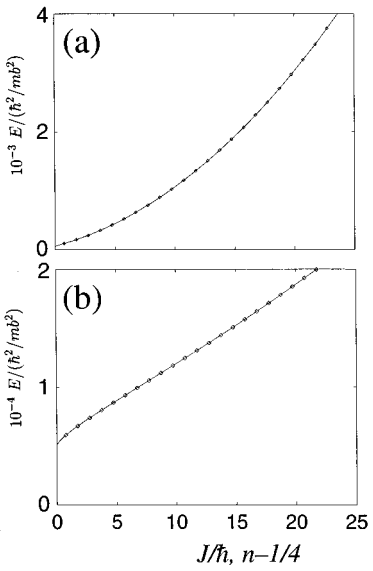

FIG. 1. Energies $E_{l,n}$ and $E_L^{\rm cl}(J)$ from quantum and classical mechanics with respect to the quantum number n and the action J, respectively. (a) $L=10\hbar$. (b) $L=100\hbar$. Solid curves $E=E_L^{\rm cl}(J)$ show classical results and points ($\diamond$) $E=E_{l,n}$ show quantum results.

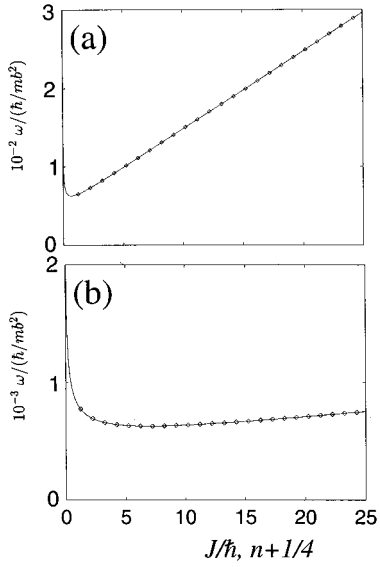

FIG. 2. Frequencies $\omega_{l,n}=(E_{l,n+1}-E_{l,n})/\hbar$ and $\omega_L^{\rm cl}(J)=dE_L^{\rm cl}(J)/dJ$ from quantum and classical mechanics with respect to the quantum number n and the action J respectively. (a) $L=10\hbar$. (b) $L=100\hbar$. Solid curves $\omega=\omega_L^{\rm cl}(J)$ show classical results and points ($\diamond$) $\omega=\omega_{l,n}$ show quantum results.

The energy eigenvalue problem in real space is given by

$$\left[-\frac{\hbar^2}{2m}\frac{\partial^2}{\partial r^2}-\frac{\hbar^2}{2mr}\frac{\partial}{\partial r}-\frac{1}{2mr^2}\frac{\partial^2}{\partial\phi^2}+V_a(r)+V_b(r)\right]\times\langle r,\phi|l,n\rangle=E_{l,n}\langle r,\phi|l,n\rangle, \tag{3}$$

with the energy eigenstates

$$\langle r,\phi|l,n\rangle=\frac{\sqrt{2}}{bJ_{l+1}(\alpha_{l,n}/b)}\ J_l\left(\frac{\alpha_{l,n}r}{b}\right)\frac{1}{\sqrt{2\pi}}e^{il\phi} \tag{4}$$

for $|l|\geqslant 1$ and $n\geqslant 1$. The energy eigenvalues are $E_{l,n}=(\hbar^2/mb^2)(\alpha_{l,n}^2/2)$, where $\alpha_{l,n}$ is the nth zero of $J_l(x)$, the Bessel functions of the first kind. (States with $l=0$ are excluded due to the boundary condition of our model $\Psi|_{r=0}=0$. We assume $a\simeq 0$.)

This system may also be studied classically [5], and some key results are summarized in the Appendix. We can compare the energy eigenvalues $E_{l,n}$ for the quantum system with the energy $E_L^{\rm cl}(J)$ of a classical particle in the circular cavity, where J is the classical action defined in the Appendix. The quantization condition from the semiclassical theory $J=(n-\frac{1}{4})\hbar$ is used [6] to get the relation between the classical action J and the quantum number n. In Fig. 1 we compare classical and quantum energies for angular momenta $L=10\hbar$ and $L=100\hbar$, respectively. They agree to very good accuracy even at low energies where $|l|$ and n are small. We can also compare the quantum frequencies $\omega_{l,n}\equiv(E_{l,n+1}-E_{l,n})/\hbar$ with the classical natural frequency $\omega_L^{\rm cl}(J)=dE_L^{\rm cl}(J)/dJ$. In Fig. 2 we compare classical and quantum frequencies for angular momenta $L=10\hbar$ and $L=100\hbar$, respectively. Since the action variable can take on a continuous range of values, the classical frequency will always have a minimum value. It is this feature that allows a bifurcation and creation of new resonances as the frequency of the magnetic flux is varied. From Fig. 2 we see that the quantum system will not always have a minimum because the action variable is quantized. For angular momentum $L=10\hbar$ the classical minimum lies below the lowest quantum state so no bifurcation can occur in the quantum system. However, for angular momentum $L=100\hbar$ there is hope of seeing a bifurcation in the quantum system because the minimum does exist.

Let us define an energy $\overline{E_L}$ such that, for the electron with the angular momentum $L=l\hbar$ the frequency $\omega_L^{\rm cl}(J)$ has a minimum value $\omega_{L,\min}$ at energy $E=\overline{E_L}$. From the quantum energy eigenvalues, we find that for $1\leqslant|l|\leqslant 11$, $E_L<E_{l,1}$; for $12\leqslant|l|\leqslant 25$, $E_{l,1}<E_L<E_{l,2}$; for $26\leqslant|l|\leqslant 40$, $E_{l,2}<E_L<E_{l,3}$, and so on. Thus the location of $\overline{E_L}$ shifts to higher-energy states as $|l|$ is increased.

B. Full Hamiltonian ($\beta\neq 0$)

The full Schrödinger equation is given in Eq. (1). We can write the full Hamiltonian in the form

$$\hat{H}(t)=\hat{H}_0-\beta\frac{\hat{p}_\phi}{m\hat{r}^2}\cos(\omega_0 t)+\beta^2\frac{1}{2m\hat{r}^2}\cos^2(\omega_0 t). \tag{5}$$

The full Hamiltonian has two perturbation terms: one proportional to β with frequency ω_0 and another proportional to β^2 with frequency $2\omega_0$. Since $[\hat{H},\hat{p}_\phi]=0$, the angular momentum is still a constant of motion and the radial and angular motions remain decoupled. However, the radial motion now is affected by a time-periodic potential energy that contains two different frequencies ω_0 and $2\omega_0$.

In Ref. [5] we found for the classical system that the resonance condition for the νth primary resonance due to the β term is $\omega_0=\nu\omega_L^{\rm cl}(J)$. Similarly, the resonance condition

for the νth primary resonance due to the β^2 term is $\omega_0=(\nu/2)\omega_L^{\rm cl}(J)$. Let $\omega_{L,\min}$ denote the minimum value of the classical frequency $\omega_L^{\rm cl}(J)$, i.e., the point where the bifurcation can occur. Then, if $\omega_0<\frac{1}{2}\omega_{L,\min}$, there is no primary resonance and as ω_0 reaches $\frac{1}{2}\omega_{L,\min}$ the primary resonance due to the β^2 term starts to emerge and bifurcate immediately [$\omega_0=\frac{1}{2}\omega_L^{\rm cl}(J)$ has two solutions if $\omega_0>\frac{1}{2}\omega_{L,\min}$]. Furthermore, if ω_0 reaches $\omega_{L,\min}$, the primary resonance due to the β term starts to emerge.

In the quantum system, as we saw in Fig. 2, if $|l|$ is small a bifurcation cannot occur because $\omega_{l,n}$ does not have two branches. On the other hand, for large $|l|$, we can expect that the bifurcation process exists in quantum mechanics. We can view this as a kind of suppression of resonances due to the finiteness of $\hbar$. (For fixed L, the smaller $\hbar$, the larger l.)

In order to see this bifurcation process occur in the quantum system, we will compute the Floquet eigenstates and show their behavior in the classical phase space using Husimi distribution functions [7]. The procedure to obtain Floquet states is as follows. The full time-periodic Hamiltonian $\hat{H}(t)$ [$\hat{H}(t)=\hat{H}(t+T_0)$ with $T_0=2\pi/\omega_0$] can be represented in the basis $\{|l,n\rangle\}$,

$$\hat{H}(t)=\sum_{l,n}\sum_{l',n'}H^l_{nn'}(t)\,\delta_{l,l'}|l,n\rangle\langle l',n'|, \tag{6}$$

where

$$H^l_{nn'}(t)=\left(\frac{\hbar^2}{2mb^2}\right)\{\alpha^2_{ln}\delta_{nn'}-c^l_{nn'}[2l\widetilde{\beta}\,\cos(\omega_0 t) -\widetilde{\beta}^2\cos^2(\omega_0 t)]\}, \tag{7}$$

with $L=l\hbar$, $\beta=\widetilde{\beta}\hbar$, and

$$c^l_{nn'}\equiv\frac{\sqrt{2}}{J_{l+1}(\alpha_{ln})J_{l+1}(\alpha_{ln'})}\int_0^1 dx\; J_l(\alpha_{ln}x)J_l(\alpha_{ln'}x)/x.$$

In order to compute the Floquet states numerically we must truncate this matrix, but we can do it in such a manner that the results we are interested in are not affected. In terms of the $N\times N$ truncated matrix, the Schrödinger equation becomes

$$i\hbar\frac{d}{dt}\Psi^l_n(t)=\sum_{n'=1}^{N}H^l_{nn'}(t)\Psi^l_{n'}(t), \tag{8}$$

where $\Psi^l_n(t)=\langle l,n|\Psi(t)\rangle$. We integrate the equation N times from $t=0$ to $t=T_0$ with initial conditions $|\Psi(t=0)\rangle=|l,n\rangle$ ($1\leqslant n\leqslant N$). Each integration gives us one column of the matrix representation of the evolution operator $\hat{U}(T_0)$, which satisfy the equation

$$|\Psi(t=T_0)\rangle=\hat{U}(T_0)|\Psi(t=0)\rangle. \tag{9}$$

Eigenvectors of this unitary operator are the Floquet states $|\Psi^l_{F,\alpha}\rangle$, which satisfy

$$\hat{U}(T_0)|\Psi^l_{F,\alpha}\rangle=e^{i\Omega_\alpha T_0}|\Psi^l_{F,\alpha}\rangle, \tag{10}$$

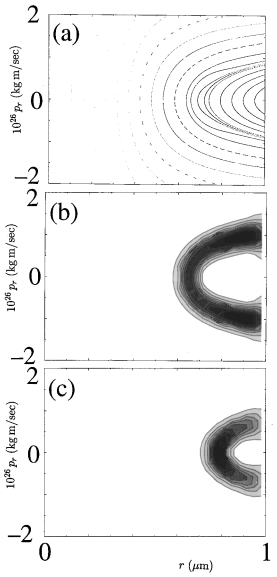

FIG. 3. $m=0.067m_e$, $b=1$ μm, $\beta=5\hbar$, $L=100\hbar$, and $\omega_0=0.9973(\omega_{L,\min}/2)$. $\omega_{L,\min}/2=5.428\times10^{11}$ Hz in this case. (a) Classical strobe plot. (b) and (c) Husimi plots with $d=0.0309$ μm.

where Ω_α is the Floquet eigenvalue, sometimes called the quasienergy. After solving the eigenvalue problem, we have representations of N Floquet states $\langle l,n|\Psi^l_{F,\alpha}\rangle$ ($1\leqslant\alpha\leqslant N$). ($\langle l,n|\Psi^l_{F,\alpha}\rangle$ obtained from the truncated Hamiltonian is a good approximation only if $\langle l,n|\Psi^l_{F,\alpha}\rangle$ has all its support on states $|l,n\rangle$ with $n<N$.) For each Floquet eigenstate $|\Psi^l_{F,\alpha}\rangle$, we can compute the Husimi distribution function

$$F^l_\alpha(r_0,p_{r0})\equiv|\langle r_0,p_{r0};l|\Psi^l_{F,\alpha}\rangle|^2, \tag{11}$$

where $|r_0,p_{r0};l\rangle=|r_0,p_{r0}\rangle|l\rangle$, $|r_0,p_{r0}\rangle$ is a coherent state, which in the position representation has the form

$$\langle r|r_0,p_{r0}\rangle=\frac{1}{\sqrt{r}}\left(\frac{1}{2\pi d^2}\right)^{1/4} \times\exp\left(-\frac{(r-r_0)^2}{4d^2}+\frac{i}{\hbar}p_{r0}(r-r_0)\right), \tag{12}$$

and $|l\rangle$ is an eigenstate of $\hat{p}_\phi$. Thus the coherent state is a Gaussian wave packet in (r,p_r) space centered at (r_0,p_{r0}) with dispersions $\Delta r=d$, and $\Delta p_r=\hbar/2d$. We should note that the use of $\langle r|r_0,p_{r0}\rangle$ for a system with hard walls does not accurately represent the system very near the hard wall. However, it is not a serious problem if $d/b\ll1$ unless r_0 is close to the wall. Then, an appropriate choice of d is important in the Husimi plots. For all Husimi plots in this paper, d was chosen to make the lengths of the dispersions $\Delta r=d$ and $\Delta p_r=\hbar/2d$ the same. The ratio d/b was about 0.03 for all Husimi plots in this paper. The values of $F^l_\alpha(r_0,p_{r0})$ near the walls are not reliable. However, due to the boundary conditions, the Floquet states go to zero at the walls and therefore $F^l_\alpha(r_0,p_{r0})$ also goes to zero at the walls so the difficulty with coherent states near the walls is not a serious problem.

In Figs. 3–5, we observe the emergence and bifurcation

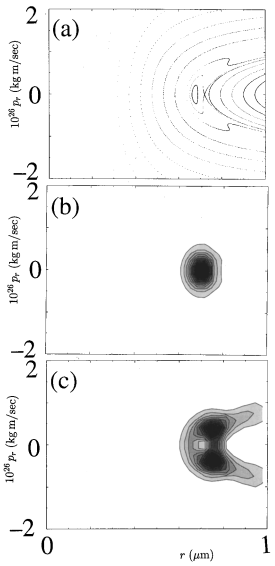

FIG. 4. $m=0.067m_e$, $b=1$ μm, $\beta=5\hbar$, $L=100\hbar$, and $\omega_0=1.001(\omega_{L,\min}/2)$. $\omega_{L,\min}/2=5.428\times10^{11}$ Hz in this case. (a) Classical strobe plot. (b) and (c) Husimi plots with $d=0.0309$ μm.

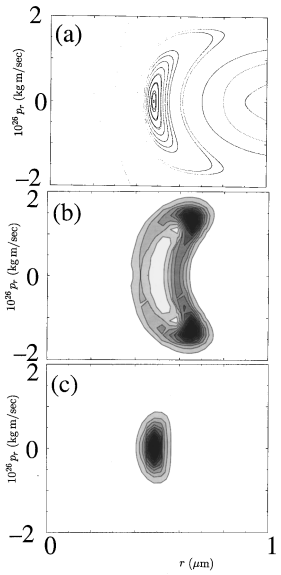

FIG. 6. Example of the first primary resonance due to the β term when $m=0.067m_e$, $b=1$ μm, $\beta=5\hbar$, $L=100\hbar$, and $\omega_0=1.155\omega_{L,\min}=6.269\times10^{11}$ Hz. (a) Classical strobe plot. (b) and (c) Husimi plots with $d=0.0309$ μm.

of primary resonances due to the β^2 term when $L=100\hbar$ as ω_0 increases near $\frac{1}{2}\omega_{L,\min}$ in both classical and quantum mechanics. In these figures, we have shown three cases $\omega_0=0.9973(\omega_{L,\min}/2)$ (Fig. 3). $\omega_0=1.001(\omega_{L,\min}/2)$ (Fig. 4), and $\omega_0=1.008(\omega_{L,\min}/2)$ (Fig. 5). (We use numbers applicable to microstructures formed at the interface between GaAs and $Al_xGa_{1-x}As$: $m=0.067m_e$, $b=1$ μm, and $\omega_{L,\min}=2\pi L/mb^2=1.086\times10^{12}$ Hz when $L=100\hbar$, where m_e is the mass of the bare electron.) Classical strobe plots show how bifurcation occurs continuously. On the other hand, the Husimi plots are not as clear as strobe plots. However, we can observe the quantum counterpart of classical results, i.e., we can find a corresponding classical orbit in the strobe plot for each Husimi plot of a Floquet state. For each case (Figs. 3–5), we choose two Floquet states that represent the case best. For the case of $\omega_0=0.9973(\omega_{L,\min}/2)$, Floquet states in Figs. 3(b) and 3(c) correspond to distorted orbits in Fig. 3(a), which shows no resonance zone. For the case of $\omega_0=1.001(\omega_{L,\min}/2)$, we observe a resonance zone has emerged. The Floquet state in Fig. 4(b) corresponds to the unstable fixed point near ($r=0.7$ μm, $p_r=0$) and the Floquet state in Fig. 4(c) corresponds to an orbit surrounding that point. They both come from the same resonance zone (both are mixed states of $|l=100,\ n=4\text{–}6\rangle$ mostly). On the other hand, the case of $\omega_0=1.008(\omega_{L,\min}/2)$ has two separate resonance zones. The Floquet state in Fig. 5(b) (mixed state of $|l=100,\ n=8\text{–}12\rangle$ mostly) corresponds to the stable fixed point near ($r\simeq0.65$ μm, $p_r=0$) in Fig. 5(a) and the Floquet state in Fig. 5(c) (mixed state of $|l=100,\ n=4\text{–}6\rangle$ mostly) corresponds to the stable fixed points near ($r=1$ μm, $p_r\simeq\pm0.95\times10^{-26}$ kg m/sec) in Fig. 5(a). We can say that the resonance zone for the quantum system has bifurcated as it does for the classical case. There was no bifurcation when $L=10\hbar$ as expected (plots are not shown in

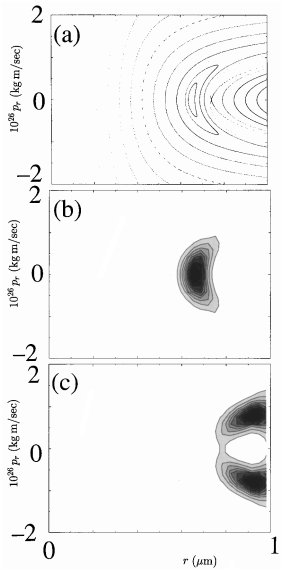

FIG. 5. $m=0.067m_e$, $b=1$ μm, $\beta=5\hbar$, $L=100\hbar$ and $\omega_0=1.008(\omega_{L,\min}/2)$. $\omega_{L,\min}/2=5.428\times10^{11}$ Hz in this case. (a) Classical strobe plot. (b) and (c) Husimi plots with $d=0.0309$ μm.

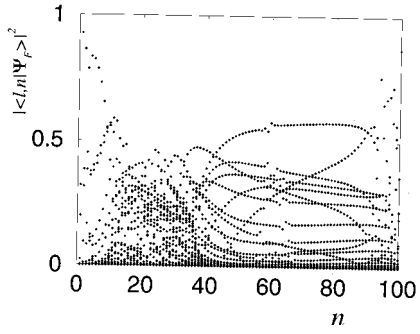

FIG. 7. Collection of probability distribution of Floquet states $(|\langle l,n|\Psi^l_{F,\alpha}\rangle|^2$ vs n for $1\leqslant\alpha\leqslant100)$.

this paper) because as we show in Fig. 2(a), there are no quantum states available to support the resonance.

For the later use, we also look at an example of the first primary resonance due to the β term when $L=100\hbar$ and $\omega_0=1.155\omega_{L,\min}=725.7(\hbar/mb^2)$. From the equation $\omega_0=\omega_L^{\rm cl}(J)$, we can find that near $J\simeq 21\hbar$ $(n\simeq 21)$ we have a resonance zone. [See Fig. 2(b).] In Fig. 6 we observe classical and quantum resonances for this case. Figure 7 is the diagram that is the collection of probability distributions of all Floquet states $(1\leqslant\alpha\leqslant 100)$ with the basis $\{|l,n\rangle, 1\leqslant n\leqslant 100\}$. It enables us to look at the states globally as we do in classical strobe plots. For example, we can distinguish irregular and regular zones; near $n\simeq 21$ we have a resonance zone with the width of about 20 and there is another small resonance zone near $n\simeq 60$ that is a fractional resonance satisfying the resonance condition $\omega_L^{\rm cl}(J)=\frac{3}{2}\omega_0$. We will ignore the scatter of points for $n>90$ because the truncation error is not small in that region.

The half-width (ΔJ) of each νth primary resonance due to the β term can be calculated approximately classically [8] by introducing the Hamiltonian that isolates the resonance term,

$$H^{\rm cl}(J,\theta)\simeq H_0(J)+V(J)\cos(\nu\theta-\omega_0 t). \tag{13}$$

Then the half-width of this resonance at $J=J'$ is approximately

$$(\Delta J)\simeq 2\sqrt{|V(J')|[d\omega(J)/dJ]^{-1}_{J=J'}}, \tag{14}$$

where $\omega(J)=dH_0(J)/dJ$.

For our model, $V(J)=-(L\beta/2m)b_\nu(E_L^{\rm cl}(J),L)$,

$$b_\nu(E,L)=\frac{2mE}{\pi}\int_{-\pi}^{\pi}\frac{d\theta\,\cos(\nu\theta)}{L^2+\theta^2(2mb^2E-L^2)/\pi^2},$$

and $\omega(J)=\omega_L^{\rm cl}(J)$. For the case in Fig. 6, we have $\nu=1$, $\beta=5\hbar$, $L=100\hbar$, and $J'=21\hbar$; then the half-width (ΔJ) is about 12, which matches well the result in Fig. 7.

III. TWO-DIMENSIONAL ELECTRON GAS

The system we describe in Sec. II might possibly be realized in the laboratory at a semiconductor interface where a two-dimensional electron gas can form. The circular outer walls of radius b are formed at the interface with metallic gates to which a negative voltage is applied. At sufficiently low temperatures the motion of the electrons will be ballistic. They will not experience impurities. In this circular system, our model has a fiber with negligible radius containing a confined magnetic flux $\Phi_0\cos(\omega_0 t)$, which provides the vector potential and the boundary condition at $r=0$.

It is useful to consider parameters appropriate for a micrometer-size semiconductor device. We choose the electron density to be $n_e=6.4\times 10^{15}$ m^{-2}, the radius $b=1$ μm, and electron effective mass $m=0.067m_e$, where m_e is the mass of the electron. The Fermi energy ϵ_F of the two-dimensional electron gas is

$$\epsilon_F=\frac{\pi\hbar^2}{m}n_e\equiv\left(\frac{\hbar^2}{mb^2}\right)N_e, \tag{15}$$

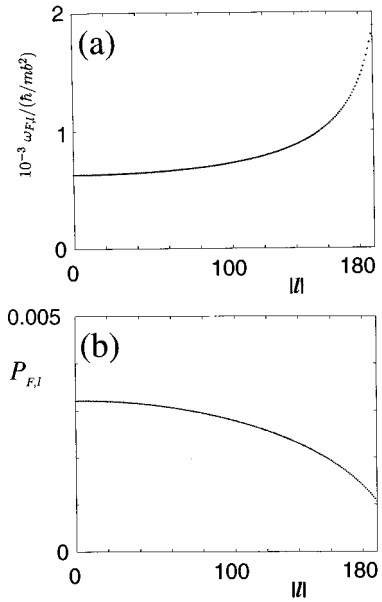

FIG. 8. When $b=1$ μm, the Fermi energy ϵ becomes $(\hbar^2/mb^2)(2.0\times 10^4)$. l_F is 189. (a) $\omega_{F,l}$ (the natural frequency of Fermi electrons with respect to l), and (b) $P_{F,l}\equiv N_{F,l}/N_F$ (the fraction of Fermi electrons with angular momentum $l\hbar$, which can be interpreted as the probability of finding Fermi electrons with the angular momentum $l\hbar$ within all Fermi electrons). $N_F\equiv\Sigma_{-l_F}^{l_F}N_{F,l}$.

where N_e can be regarded as the total number of electrons in the system (2×10^4 for the system considered here with $\epsilon_F=3.6\times 10^{-21}$ J). For a given Fermi energy ϵ_F there is an upper limit l_F of the angular momentum $|l|$ because the ground-state energy for a given l, $E_{l,1}=(\hbar^2/mb^2)(\alpha_{l,1}^2/2)$, should be smaller than the Fermi energy $\epsilon_F=(\hbar^2/mb^2)N_e$. Therefore, l_F is the largest l that satisfies the relation $\alpha_{l,1}^2<2N_e$. For our system, $l_F\simeq 189$.

We are interested in electrons with energies E near the Fermi energy (hereafter referred to as Fermi electrons) that satisfy $\epsilon_F-\Delta E/2\leqslant E\leqslant\epsilon_F+\Delta E/2$ with $\Delta E\sim k_BT$. Therefore, unlike the analysis in Sec. II, we are varying the angular momentum with fixed energy. Below we will obtain two equations using classical formulas based on the fact that the quantum results agrees very well with classical results even with low-energy states.

The frequency $\omega_{F,l}$ of a Fermi electron as a function of l can be obtained using the classical formula $\omega_L^{\rm cl}J(E)=2\pi E/\sqrt{2mb^2E-L^2}$ (cf. Ref. [5] or the Appendix),

$$\omega_{F,l}\equiv\omega_{L=l\hbar}^{\rm cl}(E=\epsilon_F)=\left(\frac{\hbar}{mb^2}\right)\frac{2\pi N_e}{\sqrt{2N_e-l^2}}. \tag{16}$$

This function is plotted in Fig. 8(a).

The number $N_{F,l}$ of Fermi electrons as a function of l can be obtained using two relations. It is proportional to the number of states at the Fermi surface so $N_{F,l}\propto(\Delta J)_l$. But $(\Delta J)_l\propto\Delta E(dE_L^{\rm cl}(J)/dJ)^{-1}$, $\Delta E\sim k_BT$ for any l, and $(dE_L^{\rm cl}(J)/dJ)_{E=\epsilon_F}=\omega_{F,l}$. Therefore,

$$N_{F,l} \propto \frac{1}{\omega_{F,l}} \propto \sqrt{\frac{2N_e - l^2}{N_e}}. \tag{17}$$

The fraction of Fermi electrons with angular momentum $l\hbar$ is plotted in Fig. 8(b).

Interestingly, it is always true that $\omega_{F,l} \geqslant \omega_{L,\min}$ [$\omega_{L=l\hbar,\min} = (\hbar/mb^2)2\pi l$ and this is an equality if $l = \sqrt{N_e}$], which can mean that when $\omega_0 \simeq \nu\omega_{F,l}$, the νth primary resonance due to the β term can occur for the Fermi electrons with the angular momentum $l\hbar$. Therefore, we can find the critical frequency $\omega_{\rm cr}$,

$$\omega_{\rm cr} \equiv \omega_{F,l=0} = \left(\frac{\hbar}{mb^2}\right)\pi\sqrt{2N_e} \tag{18}$$

such that when ω_0 is lower than $\omega_{\rm cr}$, no Fermi electron has a primary resonance due to the β term. (There exist Fermi electrons that have a primary resonance due to the β^2 term satisfying $\omega_0 = \frac{1}{2}\omega_{F,l}$ when $\omega_{\rm cr}/2 < \omega_0 < \omega_{\rm cr}$. But, from here on, we will ignore primary resonances due to the β^2 term assuming that β is small enough.) As ω_0 reaches $\omega_{\rm cr}$, the first primary resonance due to the β term starts to occur at $l=1$. (In the model discussed here, states with $l=0$ have been excluded due to the boundary condition provided by the fiber.) If ω_0 increases further, Fermi electrons with different l (satisfying $\omega_0 = \omega_{F,l}$) have primary resonances. Also, when ω_0 is larger than $2\omega_{\rm cr}$, two kinds of primary resonances will start to exist, one at $l=l'$ (the second primary resonance $\omega_0 = 2\omega_{F,l'}$) and the other at $l=l''$ (the first primary resonance $\omega_0 = \omega_{F,l'}$).

For example, if $\omega_0 = 1.254\times10^{12}$ Hz (which satisfies $\omega_0 \simeq \omega_{F,l=100}$ and $\omega_0 = 1.155\omega_{L=100\hbar,\min} = 1.155\omega_{\rm cr}$), Fermi electrons with $l \simeq 100$ will have the first primary resonance due to the β term. In Fig. 6 we showed classical and quantum results for this particular resonance. We can obtain an estimate of the range of the angular momenta Δl that participate in the resonance. Using Eq. (14), $\Delta\omega \simeq \Delta J(d\omega/dJ)$, and $\Delta l \simeq 2\Delta\omega(d\omega_{F,l}/dl)^{-1}_{l=l'}$, we can get $\Delta l \sim 20\sqrt{\tilde{\beta}}$. Then we can say that the range of l is proportional to $\sqrt{\beta}$ when β is small and that Fermi electrons with the angular momenta, $l\hbar$, when l satisfies $|l-l'| \leqslant \Delta l/2$ with $\omega_0 = \nu\omega_{F,l'}$, are in their νth primary resonance zones.

IV. DISCUSSION AND CONCLUSIONS

We have studied the model of a 2D electron gas in a circular cavity with hard walls and a weak time-periodic radial potential. We have seen that the quantum chaotic behavior of our model corresponds well with classical results when the angular momentum is large. We have observed emergence and bifurcation of primary resonances, which can be characterized by irregular mixing of Floquet states, and we have also observed them in the Husimi plots. Husimi plots matched classical strobe plots very well except in the region near the infinitely hard walls. Husimi distribution functions go to zero near walls due to the boundary condition. One of the consequences is that fixed points that reside on the walls in classical strobe plots cannot be seen in the Husimi plots.

We viewed the problem as a noninteracting Fermi gas. We discussed some properties of the electrons at the Fermi surface as a function of the angular momentum. For a given Fermi energy, the angular momentum has an upper limit and the natural frequency of an electron has a minimum $\omega_{\rm cr}$ at which the angular momentum is zero. If the external frequency ω_0 is smaller than $\omega_{\rm cr}$, there is no electron having a primary resonance. If ω_0 is larger than $\omega_{\rm cr}$, electrons with certain angular momenta will have primary resonances.

These results might be of interest for conductance studies in semiconductor microstructures such as high-mobility GaAs-$Al_xGa_{1-x}As$ heterostructures at low temperature since this system exhibits a controlled transition to chaos. In that case, phonon-electron scattering and impurity scattering can be neglected because their mean free paths are known to be much longer than the size of the system ($\sim 1\,\mu$m) [9]. We can also neglect Coulomb interactions (when $T \sim 1$ K, the mean free path is theoretically on the order of 10^2 μm in the system given in Sec. III [10]).

ACKNOWLEDGMENTS

The authors wish to thank the Welch Foundation, Grant No. 1051, for partial support of this work, and the University of Texas High Performance Computing Center for use of its facilities. The authors also wish to thank Sukkeun Kim for his help on computer programs.

APPENDIX: CLASSICAL RESULTS

In this appendix we briefly review the classical results [5]. We treat electromagnetic waves classically in our model because ω_0 is low. The exact form of the vector potential after solving Maxwell's equations is

$$\mathbf{A}(r,t) = \frac{\Phi_0}{\pi a^2}\frac{J_1(ka)[N_1(kr)\cos(\omega_0 t) - J_1(kr)\sin(\omega_0 t)]}{J_0(ka)N_1(ka) - J_1(ka)N_0(ka)}\mathbf{e}_\phi \tag{A1}$$

in the region $a < r < b$ (where $k = \omega_0/c$). If ω_0 is low enough to satisfy $kb \ll 1$, the vector potential takes the form $\mathbf{A}(r,t) \simeq (\Phi_0/2\pi r)\cos(\omega_0 t)\mathbf{e}_\phi$ by using the asymptotic forms of Bessel functions.

The classical Hamiltonian becomes

$$H^{\rm cl}(t) = \frac{p_r^2}{2m} + \frac{[p_\phi - \beta\cos(\omega_0 t)]^2}{2mr^2} + V_a(r) + V_b(r), \tag{A2}$$

where $\beta = e\Phi_0/2\pi$, and V_a and V_b are the potentials associated with the infinitely hard walls at $r=a$ and $r=b$. Since ϕ is a cyclic coordinate, we can let $p_\phi = L$ and we view this system as the system with one degree of freedom with time dependence (1.5 degrees of freedom).

Now let us consider $H_0^{\rm cl}$, which is the free Hamiltonian

$$H_0^{\rm cl}(r,p_r) = \frac{p_r^2}{2m} + \frac{L^2}{2mr^2} + V_a(r) + V_b(r). \tag{A3}$$

It is useful to obtain a canonical transformation from (r,p_r) to the action-angle variable (J,θ), where J is given by

$$J=\frac{1}{2\pi}\oint p_r dr=\frac{\sqrt{2mE}}{\pi}\left[\sqrt{b^2-\frac{L^2}{2mE}}-\frac{L}{\sqrt{2mE}}\cos^{-1}\left(\frac{L}{b\sqrt{2mE}}\right)\right]. \quad \text{(A4)}$$

Then, with H_0 as a function of J, $E_L^{\rm cl}(J)$ can be obtained by solving Eq. (A4) as a function of J. The natural frequency of the motion is

$$\omega_L^{\rm cl}(J)=\dot{\theta}=\frac{dE_L^{\rm cl}(J)}{dJ}\quad\left(=\frac{2\pi E}{\sqrt{2mb^2E-L^2}}\right), \quad \text{(A5)}$$

so $\omega_L^{\rm cl}$ has a minimum $\omega_{L,\min}(=2\pi L/mb^2)$ at $E=E_L$ $(=L^2/mb^2)$.

Let us now write the full Hamiltonian in terms of (J,θ),

$$H^{\rm cl}(t)=E_L^{\rm cl}(J)-\beta\frac{L}{2m}\sum_{\nu_1=-\infty}^{\infty}b_{\nu_1}(J)\cos(\nu_1\theta-\omega_0 t)+\beta^2\frac{1}{8m}\sum_{\nu_2=-\infty}^{\infty}b_{\nu_2}(J)\cos(\nu_2\theta-2\omega_0 t)+\beta^2\frac{1}{4m}r^{-2}(J,\theta), \quad \text{(A6)}$$

where b_ν is the coefficient of the Fourier cosine series of $r^{-2}(J,\theta)$ and is given by

$$b_\nu(J)=b_\nu(E,L)=\frac{2mE}{\pi}\int_{-\pi}^{\pi}\frac{d\theta\cos(\nu\theta)}{\left[L^2+\frac{\theta^2}{\pi^2}(2mb^2E-L^2)\right]}.$$

The two sets of traveling cosine waves in Eq. (A6) give rise to infinite sets of primary resonances in the phase space. The cosine waves that are proportional to β give rise to resonance zones that dominate the phase space for small β. On the other hand, those proportional to β^2 give rise to resonance zones that dominate the phase space for large β. There are also two sets of resonance conditions; $\omega_0=\nu\omega_L^{\rm cl}(J)$ for primary resonances due to the β term and $\omega_0=(\nu/2)\omega_L^{\rm cl}(J)$ for primary resonances due to the β^2 term. Action variables J that satisfy those conditions locate the positions of the νth primary resonances in (J,θ) space [and therefore in (r,p_r) space]. Finally, the fact that $\omega_L^{\rm cl}(J)$ has a minimum value $\omega_{L,\min}$ means that if ω_0 is lower than $\omega_{L,\min}/2$ there is no primary resonance and as ω_0 reaches $\omega_{L,\min}/2$ we can observe emergence and bifurcation of the primary resonance due to the β^2 term.

[1] G.O. Morrow and L.E. Reichl, Phys. Rev. A **50**, 2027 (1994).
[2] S.J. Chang and K.J. Shi, Phys. Rev. A **34**, 7 (1986).
[3] L.E. Reichl, *The Transition to Chaos In Conservative Classical Systems: Quantum Manifestations* (Springer-Verlag, New York, 1992).
[4] H. Sambe, Phys. Rev. A **7**, 2203 (1973).
[5] S. Ree and L.E. Reichl, Phys. Rev. E **53**, 1228 (1996).
[6] J.J. Sakurai, *Modern Quantum Mechanics* (Addison-Wesley, Reading, MA, 1985), see the quarkonium example on p. 108.
[7] K. Husimi, Proc. Phys. Math. Soc. (Jpn.) **22**, 246 (1940).
[8] B.V. Chirikov, Phys. Rep. **52**, 263 (1979).
[9] A. Yacobi, U. Siban, C.P. Umbach, and J.M. Hong, Phys. Rev. Lett. **66**, 1938 (1991); C.M. Markus, R.M. Westerfelt, P.F. Hopkins, and A.C. Gossard, Phys. Rev. B **48**, 2460 (1993).
[10] G.F. Giuliani and J.J. Quinn, Phys. Rev. B **26**, 4421 (1982).